J Nanostruct 16(2): 1833-1847, Spring 2026

RESEARCH PAPER

Design, Preparation, and Characterization of L-Glutamic Acid Functionalized Graphene Oxide (GO-L-Glu) for Application in Targeted Cancer Therapy

Asokan Vasudevan [1]*, Uday Abdul-Reda Hussein [2], Ayser Imad Abdul-aziz [3], Khalid Ibrahim Adwan [4], Mahmood Hasen Shuhata [5], Safa Jasim Tuama [6], Suleiman Ibrahim Mohammad [7], Xujabayev Safarboy [8], Xurshid Axmedov [9], Esanov Dilshod [9], Dilnoza Saidjalilova [10], Axmadulina Galiya [11], Nargiza Abdurakhmanova [12], Abdukodirov Sherzodjon [13]

[1] *Faculty of Business and Communications, INTI International University, 71800 Negeri Sembilan, Malaysia*

[2] *Department of Pharmaceutics, College of Pharmacy, University of Al-Ameed, Iraq*

[3] *Department of Pharmacy, Al-Turath University, Baghdad, Iraq*

[4] *Department of Pharmacy, College of Pharmacy, Al-Nisour University, Baghdad, Iraq*

[5] *Al-Hadi University College, Baghdad, Iraq*

[6] *College of Health and Medical Technologies, National University of Science and Technology, Dhi Qar, Iraq*

[7] *INTI International University, 71800 Negeri Sembilan, Malaysia*

[8] *Department of General Surgery, Samarkand State Medical University, Samarkand 140100, Uzbekistan*

[9] *Department of Orthopedic Dentistry and Orthodontics, Bukhara State Medical Institute, Bukhara, Uzbekistan*

[10] *Department of Obstetrics and Gynecology, Reproductology, Tashkent State Medical University, Tashkent, Uzbekistan*

[11] *Axmadulina Galiya - Department of Therapeutic Sciences, Fergana Medical Institute of Public Health, Fergana, Uzbekistan*

[12] *Department of Fashion Design, Tashkent Institute of Textile and Light Industry, Uzbekistan*

[13] *Department of Infectious Diseases, Andijan State Medical Institute, Andijan, Uzbekistan*

ARTICLE INFO

Article History:
Received 05 December 2025
Accepted 25 March 2026
Published 01 April 2026

Keywords:
Cancer
Graphene oxide
L-glutamic acid
Nanomedicine
Therapy
Treatment

ABSTRACT

The development of targeted nanocarriers that selectively deliver chemotherapeutic agents to tumor cells remains a critical challenge in oncology. This study reports the rational design, synthesis, and comprehensive characterization of a novel nanoplatform based on L-glutamic acid-functionalized graphene oxide (GO-L-Glu) for targeted cancer therapy. The covalent conjugation was achieved via a carbodiimide-mediated amidation reaction, meticulously optimized to ensure high functionalization density. Advanced characterization techniques, including FT-IR and TGA, confirmed successful grafting, with TGA indicating a substantial increase in organic content. The GO-L-Glu carrier demonstrated a high loading capacity (45.7%) for doxorubicin (DOX) and exhibited a pronounced pH-responsive release profile, with 88.7% of DOX released at pH 5.0 versus only 42.5% at pH 7.4 over 72 hours. *In vitro* studies revealed that the GO-L-Glu/DOX conjugate maintained potent cytotoxicity against xCT transporter-overexpressing cancer cell lines (MDA-MB-231 and U-87 MG) while showing significantly reduced toxicity towards normal human dermal fibroblasts. A competitive inhibition assay using sulfasalazine mechanistically proved that cellular uptake occurs primarily via xCT-mediated endocytosis. Furthermore, functionalization drastically improved hemocompatibility, reducing hemolysis by more than 50% compared to pristine GO. These collective results validate GO-L-Glu as a multifunctional, safe, and highly selective nanocarrier, offering a promising strategy for targeting tumor metabolism and overcoming limitations of conventional chemotherapy.

How to cite this article
Vasudevan A., Hussein U., Abdul-aziz A. Design, Preparation, and Characterization of L-Glutamic Acid Functionalized Graphene Oxide (GO-L-Glu) for Application in Targeted Cancer Therapy. J Nanostruct, 2026; 16(2):1833-1847. DOI: 10.22052/JNS.2026.02.034

* *Corresponding Author Email: Husseinmprism@oulook.com*

INTRODUCTION

The pursuit of effective cancer therapeutics has long driven innovation at the interface of materials science and biomedicine [1-5]. Within this domain, carbon-based nanomaterials have emerged as a transformative platform over the past two decades, offering unprecedented opportunities for targeted intervention [6-11]. Following the pioneering exploration of fullerene derivatives and carbon nanotubes, graphene oxide (GO) has garnered significant attention due to its unique physicochemical portfolio, including a high surface area, facile functionalization capacity, and inherent biocompatibility [12-15]. The strategic decoration of the GO basal plane and edges with organic and biological molecules allows for the precise engineering of multifunctional nanocarriers [16-18]. These systems can be designed to address critical challenges in oncology, such as poor drug solubility, systemic toxicity, and lack of tumor selectivity [19]. By exploiting the enhanced permeability and retention (EPR) effect and enabling receptor-mediated active targeting, functionalized GO constructs hold the promise of augmenting therapeutic efficacy while mitigating adverse side effects [20-22]. This body of work builds upon a rich history of carbon allotrope research, positioning tailored graphene-based architectures as a cornerstone for the next generation of targeted drug delivery systems. Fig. 1 displays different carbon materials for application in cancer therapy.

The landscape of cancer therapy utilizing carbon-based nanomaterials has evolved remarkably from foundational proof-of-concept studies to sophisticated, multi-modal therapeutic platforms [23-25]. Recent research has decisively shifted from passive exploitation of the EPR effect to the active design of “smart” nanocarriers that respond to specific tumor microenvironment (TME) triggers, such as lowered pH, elevated glutathione (GSH) levels, or overexpressed enzymes. Graphene oxide, in particular, has served as a versatile scaffold for these advances. Cutting-edge strategies now seamlessly integrate targeted drug delivery with photothermal therapy (PTT), where GO’s strong near-infrared (NIR) absorption is harnessed for localized hyperthermia, and with photodynamic therapy (PDT) through the grafting of photosensitizers [26]. Furthermore, covalent and non-covalent bioconjugation techniques have grown increasingly precise, enabling the attachment of targeting ligands like folic acid, peptides, and antibodies with controlled orientation and density to enhance cellular uptake via receptor-mediated endocytosis [27]. A particularly promising direction involves the engineering of charge-reversal functionalities, where the surface charge of the nanomaterial switches from negative to positive upon reaching the acidic tumor milieu, thereby promoting cellular internalization [28]. These convergent advances underscore a paradigm where carbon platforms are no longer mere carriers but are intrinsic therapeutic agents and mediators of combination therapies, offering a potent tool to overcome multidrug resistance and improve therapeutic outcomes.

Despite the significant promise held by functionalized carbon nanomaterials in oncology, several persistent challenges continue to constrain their translation from laboratory settings to clinical application [29-31]. A primary limitation lies in the precise control over the surface chemistry during functionalization; heterogeneous or poorly defined conjugation can lead to inconsistent batch-to-batch performance, unreliable drug loading kinetics, and unpredictable biological interactions. Furthermore, while enhanced cellular uptake is a common goal, many targeting strategies rely on single-receptor recognition (e.g., folate receptors), which can be compromised by receptor heterogeneity across tumor types and patient populations. Another critical concern is the long-term fate of these materials *in vivo*, where incomplete biodegradation and potential off-target accumulation raise unresolved questions about systemic toxicity. Many existing designs also lack a concerted mechanism to actively promote intracellular drug release within the cancer cell, potentially limiting the therapeutic payload’s bioavailability even after successful delivery. Consequently, there remains a pressing need for novel conjugation methodologies that impart not only targeting specificity but also introduce responsive elements for controlled drug release, all while ensuring a well-defined and reproducible nanomaterial architecture [32-36].

To address these gaps, this study aims to design, synthesize, and thoroughly characterize a novel graphene oxide nanoplatform functionalized with L-glutamic acid, hypothesizing that this biomolecule will confer a dual function: firstly, by exploiting the overexpression of glutamate

transporters on certain cancer cells for enhanced and specific uptake, and secondly, by introducing a pH-responsive moiety to facilitate efficient intracellular drug release within the acidic lysosomal compartment.

MATERIALS AND METHODS

General Remarks

All chemical reagents and solvents were of analytical grade and used as received unless otherwise specified. Natural graphite powder (particle size < 45 µm), sulfuric acid (H_2SO_4, 98%), potassium permanganate ($KMnO_4$), hydrogen peroxide (H_2O_2, 30%), and L-Glutamic acid (L-Glu, ≥99%) were purchased from Sigma-Aldrich. N-Hydroxysuccinimide (NHS, 98%) and N-(3-Dimethylaminopropyl)-N'-ethylcarbodiimide hydrochloride (EDC·HCl, ≥98.0%) were obtained from TCI Chemicals. The phosphate-buffered saline (PBS) tablets (pH 7.4) were procured from Thermo Fisher Scientific. All aqueous solutions were prepared using ultrapure water (resistivity 18.2 MΩ·cm) from a Milli-Q® Integral water purification system (Merck Millipore). Graphene oxide (GO) was synthesized in-house from natural graphite powder via a modified Hummers' method, as detailed in the subsequent section. The covalent functionalization of GO with L-Glutamic acid was achieved through a carbodiimide-mediated amidation reaction, targeting the carboxyl groups present on the GO edges and defect sites. Material characterization was performed using the following apparatus. Field Emission Scanning Electron Microscopy (FE-SEM) images was acquired on a Thermo Scientific Apreo 2 S LoVac microscope operating at an accelerating voltage of 10 kV. Prior to imaging, samples were sputter-coated with a thin layer of gold using a Quorum Q150R S sputter coater to enhance conductivity. Fourier Transform Infrared (FT-IR) spectra were recorded in attenuated total reflectance (ATR) mode on a Bruker ALPHA

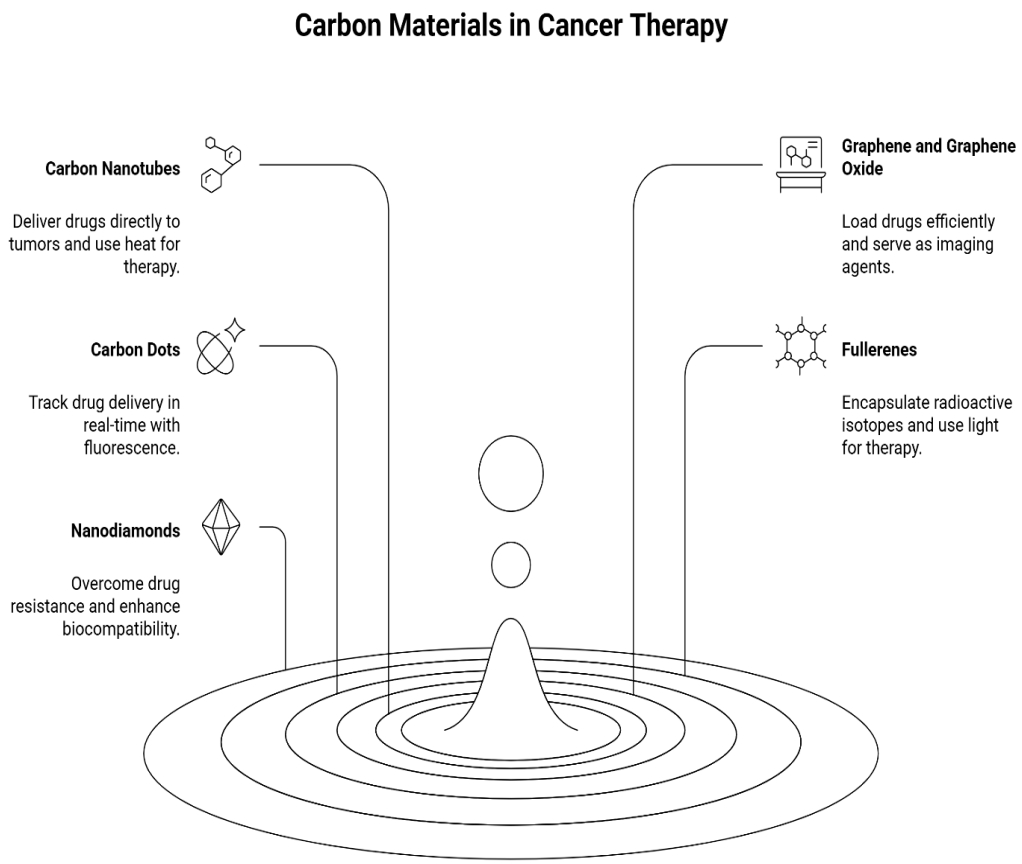

Fig. 1. Different carbon materials for application in cancer therapy.

II spectrometer equipped with a platinum ATR diamond crystal. Spectra were collected over a range of 4000 to 400 cm^{-1} with a resolution of 4 cm^{-1}, averaging 64 scans per sample to ensure a high signal-to-noise ratio. Thermal stability and the degree of functionalization were evaluated by Thermogravimetric Analysis (TGA) using a TA Instruments Discovery SDT 650. Measurements were conducted under a continuous nitrogen flow of 50 mL min^{-1}, with samples heated from room temperature to 800 °C at a constant rate of 10 °C min^{-1}.

Synthesis of (GO-L-Glu)

The covalent functionalization of graphene oxide with L-glutamic acid was accomplished via a two-step, carbodiimide-catalyzed amidation reaction, designed to conjugate the amino acid to the carboxyl groups present on the GO sheet edges and defect sites. This procedure is a modification of established protocols, optimized to maximize conjugation efficiency while preserving the nanomaterial's structural integrity. First, 100 mg of the freshly prepared graphene oxide (GO) was dispersed in 100 mL of ultrapure water and subjected to probe sonication (Sonics Vibra-Cell VCX 750, 40% amplitude) for 45 minutes in an ice bath to obtain a homogeneous, dark brown suspension (1 mg/mL). The pH of the GO dispersion was then carefully adjusted to 6.0 using dilute hydrochloric acid (0.1 M) to favor the subsequent carbodiimide chemistry. To this stirred dispersion, 240 mg (1.25 mmol) of N-(3-Dimethylaminopropyl)-N'-ethylcarbodiimide hydrochloride (EDC·HCl) and 150 mg (1.30 mmol) of N-Hydroxysuccinimide (NHS) were added sequentially. The reaction mixture was allowed to stir at room temperature under a nitrogen atmosphere for 2 hours. This step activated the carboxylic acid moieties on GO, forming unstable O-acylisourea intermediates that were stabilized by conversion to amine-reactive NHS esters.

Following the activation step, 220 mg (1.5 mmol) of L-glutamic acid (L-Glu), dissolved in 10 mL of pH 7.4 phosphate-buffered saline (PBS), was added dropwise to the reaction vessel. The PBS was employed to maintain a physiological pH conducive to the amide bond formation while ensuring the solubility of the amino acid. The resulting mixture was stirred vigorously at room temperature for 24 hours, protected from light.

Upon completion, the product, L-glutamic acid-functionalized graphene oxide (GO-L-Glu), was isolated and purified to remove unreacted reagents and byproducts. The dark suspension was centrifuged (Eppendorf 5430 R, FA-45-30-11 rotor) at 12,000 rpm for 20 minutes. The supernatant was decanted, and the obtained pellet was re-dispersed in a wash sequence of ultrapure water, followed by a 1:1 (v/v) ethanol-water mixture, and finally pure ethanol. This centrifugation-redispersion cycle was repeated five times. The final product was collected as a dark, free-flowing powder after lyophilization (Christ Alpha 1-2 LDplus freeze dryer) for 48 hours. The yield of the functionalization process was consistently found to be 85-90% by mass. A schematic representation of this synthetic route is provided in Fig. 2.

Application of L-Glutamic Acid Functionalized Graphene Oxide (GO-L-Glu) in Targeted Cancer Therapy

To evaluate the therapeutic potential and targeted delivery capability of the synthesized GO-

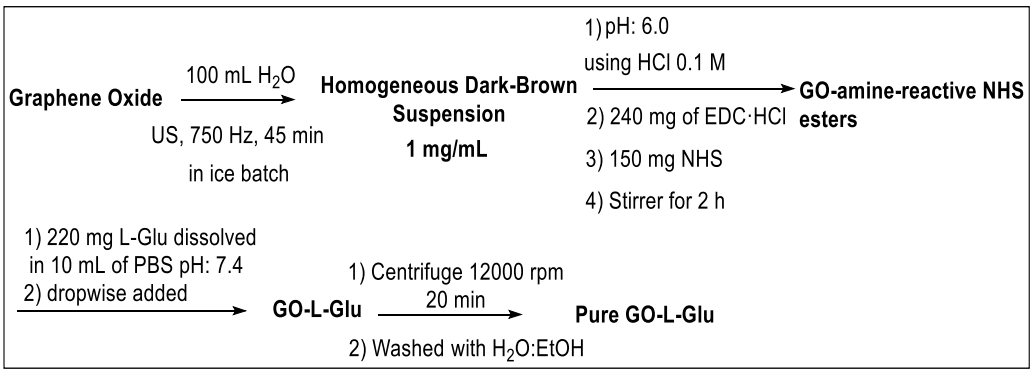

Fig. 2. The synthetic approach for preparation of GO-L-Glu.

L-Glu nanoplatform, a series of *in vitro* biological assays were designed. The central hypothesis posits that the conjugated L-glutamic acid moieties will exploit the overexpressed glutamate transporters, specifically the xCT (system xc−) transporter, on the surface of certain aggressive cancer cells, such as triple-negative breast cancer (MDA-MB-231) and glioblastoma (U-87 MG) cell lines, to facilitate enhanced and selective cellular internalization.

Drug Loading and pH-Responsive Release Profile

The anticancer drug Doxorubicin hydrochloride (DOX) was selected as a model chemotherapeutic agent. For drug loading, 10 mg of GO-L-Glu was dispersed in 10 mL of PBS (pH 7.4) and probe-sonicated for 10 minutes. A DOX solution (2 mg/mL in PBS) was added to the nanomaterial suspension at a 1:1 (w/w) ratio. The mixture was stirred in the dark at room temperature for 24 hours, relying on π-π stacking and possible electrostatic interactions between DOX and the GO-L-Glu sheets. The DOX-loaded conjugate (GO-L-Glu/DOX) was then isolated via centrifugation (14,000 rpm, 15 min) and washed with PBS until the supernatant was clear, indicating the removal of unbound drug. The loading efficiency (LE) and loading capacity (LC) were calculated spectrophotometrically by measuring the absorbance of the combined wash supernatants at 480 nm using a calibration curve and applying the formulas:

LE (%) = (Weight of loaded DOX/Weight of initial DOX) × 100

LC (%) = (Weight of loaded DOX/Weight of GO-L-Glu/DOX) × 100

The *in vitro* drug release kinetics were investigated under simulated physiological (PBS, pH 7.4) and acidic tumor microenvironment/ endosomal (acetate buffer, pH 5.0) conditions. Precisely, 5 mg of GO-L-Glu/DOX was suspended in 50 mL of the respective release medium and incubated at 37°C with constant shaking at 100 rpm. At predetermined time intervals, 2 mL aliquots were withdrawn and replaced with an equal volume of fresh pre-warmed buffer. The released DOX concentration was quantified using UV-Vis spectroscopy at 480 nm. The experiment was conducted in triplicate to ensure statistical relevance [37].

In vitro Cytotoxicity and Targeted Uptake Assessment

The biocompatibility of the blank carrier (GO-L-Glu) and the therapeutic efficacy of GO-L-Glu/DOX were evaluated using the (3-(4,5-dimethylthiazol-2-yl)-2,5-diphenyltetrazolium bromide (MTT) assay. MDA-MB-231 and U-87 MG cells, along with a non-cancerous control cell line (e.g., human dermal fibroblasts, HDF), were seeded in 96-well plates at a density of 5×10^3 cells per well and allowed to adhere for 24 hours. Cells were then treated with varying concentrations (0-100 µg/mL) of GO-L-Glu, free DOX, and GO-L-Glu/DOX for 24 and 48 hours. Following incubation, MTT reagent (0.5 mg/mL) was added, and the resulting formazan crystals were dissolved in DMSO. The absorbance was measured at 570 nm using a microplate reader (BioTek Synergy H1). Cell viability was expressed as a percentage relative to untreated control cells.

To visually confirm the hypothesized receptor-mediated uptake, a competitive inhibition assay was performed. MDA-MB-231 cells were pre-treated for 1 hour with 5 mM of sulfasalazine, a known specific inhibitor of the xCT transporter. Subsequently, both pre-treated and untreated cells were incubated with fluorescently labeled GO-L-Glu (prepared by conjugating FITC to the amino groups of L-glutamic acid prior to the main functionalization) for 4 hours. Cellular internalization was then analyzed using confocal laser scanning microscopy (CLSM, Zeiss LSM 980 with Airyscan 2) and quantified via flow cytometry (Beckman Coulter CytoFLEX S). A significant reduction in fluorescence intensity in the sulfasalazine-pre-treated group would provide direct evidence for the xCT-mediated endocytotic pathway [38].

Hemocompatibility Assay

Given the intravenous administration route proposed for such nanocarriers, a hemolysis assay was conducted using fresh human red blood cells (RBCs) to assess blood compatibility. Briefly, RBCs were separated from EDTA-treated blood, washed with sterile saline, and diluted to a 2% (v/v) suspension. This suspension was incubated with GO, GO-L-Glu, and GO-L-Glu/DOX at various concentrations (10-200 µg/mL) for 2 hours at 37°C. Sterile water and PBS served as positive (100% hemolysis) and negative (0% hemolysis) controls, respectively. After incubation, samples

were centrifuged, and the absorbance of the supernatant was measured at 540 nm to quantify released hemoglobin. The hemolysis percentage was calculated relative to the positive control [39, 40].

These combined evaluations of drug loading efficacy, pH-responsive release, selective cytotoxicity, mechanistic cellular uptake, and hemocompatibility constitute a foundational *in vitro* validation of the GO-L-Glu platform for targeted cancer therapy.

RESULTS AND DISCUSSION

Preparation and Rationale for Synthesis of L-Glutamic Acid Functionalized Graphene Oxide (GO-L-Glu)

The successful implementation of targeted drug delivery requires nanocarriers with precisely engineered surface chemistry. To this end, L-glutamic acid was covalently anchored onto graphene oxide (GO) through a carbodiimide-mediated amidation strategy, a reaction chosen for its reliability in forming stable amide linkages under aqueous conditions [41]. The synthesis, summarized in Fig. 2, was deliberately optimized to achieve high functionalization density while mitigating unwanted side reactions or GO sheet aggregation.

Initial Dispersion and pH Adjustment

The foundation of a reproducible functionalization lies in a homogeneous starting material. Probe sonication of GO in an ice bath was essential to exfoliate stacked sheets and generate a stable colloidal suspension, thereby maximizing the accessibility of surface carboxyl groups for subsequent chemistry [42]. Adjusting the pH to 6.0 prior to activation is a critical, often overlooked, step. This mildly acidic environment protonates the carboxylic acids, making them more amenable to the EDC-mediated activation mechanism, while being sufficiently high to prevent the premature hydrolysis of the NHS ester formed in the next stage [41].

Carboxyl Group Activation

The addition of EDC·HCl and NHS initiates the crucial activation sequence. EDC first reacts with a GO carboxylate to form an O-acylisourea intermediate. However, this species is susceptible to hydrolysis and rearrangement. The inclusion of NHS, in a slight molar excess, stabilizes the intermediate by converting it to a semi-stable NHS ester. This active ester is significantly more resistant to hydrolysis, providing a longer-lived electrophile for nucleophilic attack by the amine of L-glutamic acid in the subsequent step. Conducting this activation under a nitrogen atmosphere minimizes potential side reactions with atmospheric carbon dioxide [43].

Conjugation with L-Glutamic Acid: The choice of L-glutamic acid as the targeting ligand is twofold: its primary α-amine serves as the nucleophile for amide bond formation with the GO-NHS ester, while its side-chain carboxylate provides a potential handle for further modification or contributes to the material's overall hydrophilicity and charge profile. Dissolving the amino acid in PBS (pH 7.4) was intentional. This pH is optimal for the nucleophilic amine to be in its deprotonated, reactive state, driving the amidation forward, while the PBS salts help maintain ionic strength. The extended 24-hour reaction time ensures high conjugation yield by allowing the reaction to proceed to completion despite the steric hindrance presented by the GO sheet [44].

Purification and Isolation

Rigorous purification is paramount to obtaining a material free from physisorbed reagents and reaction byproducts (e.g., urea derivatives from EDC). The sequential washing regimen using water to remove salts and polar impurities, followed by aqueous ethanol and pure ethanol to displace any residual organic compounds ensures a clean product. Lyophilization, as the final step, was selected over oven drying to prevent thermal degradation and to preserve the porous, aerogel-like structure of the functionalized nanomaterial, which is beneficial for subsequent drug loading. The consistently high mass yield (85-90%) indicates efficient coupling with minimal loss of the GO backbone during processing [44, 45].

Characterization of GO-L-Glu

The morphological consequences of the covalent functionalization process were directly visualized using FE-SEM, with representative micrographs of the pristine GO and the functionalized GO-L-Glu presented in Fig. 3a and Fig. 3b, respectively.

The FE-SEM image of the unmodified GO (Fig. 3a) reveals the characteristic wrinkled, sheet-like topology associated with graphene oxide. The observed structure consists of thin, semi-

transparent flakes with lateral dimensions varying from several hundred nanometers to a few micrometers. These flakes exhibit pronounced curling and folding, a direct result of the extensive oxidation during synthesis which introduces sp^3-hybridized defects, disrupting the planar sp^2 network of graphite. The surface appears relatively smooth at this magnification, with edges that are somewhat irregular but well-defined.

A distinct morphological evolution is evident in the image of GO-L-Glu (Fig. 3b). Following functionalization with L-glutamic acid, the nanomaterial retains its fundamental two-dimensional, flake-like architecture. However, the surface texture undergoes a significant change, appearing notably more textured and coarser compared to the pristine GO. This increased surface roughness can be attributed to the successful grafting of L-glutamic acid molecules onto the GO basal plane and edges. The covalent attachment of these organic molecules disrupts the smooth, oxidized carbon surface, introducing new topological features. Furthermore, the functionalization appears to influence the packing and aggregation behavior of the sheets. While some individual flakes are still discernible, there is a tendency for increased edge-to-edge association, likely facilitated by new hydrogen bonding interactions between the carboxyl and amide groups of neighboring L-glutamic acid chains. Crucially, no evidence of large-scale, irreversible aggregation or precipitation into dense, graphitic particulates is observed, indicating that the sonication and reaction conditions successfully preserved the colloidal and nanoscopic nature of the material. This modified, rougher morphology with maintained sheet integrity is highly favorable for biomedical applications, as it provides a higher surface area for potential drug adsorption while preserving the nanoscale dimensions necessary for cellular uptake.

FT-IR spectroscopy provides direct evidence for the chemical transformations occurring during the functionalization process. The comparative spectra of pristine GO and GO-L-Glu, presented in Fig. 4a and Fig. 4b respectively, confirm the successful covalent conjugation of L-glutamic acid to the graphene oxide scaffold.

The spectrum of GO (Fig. 4a) exhibits the characteristic vibrational modes expected for highly oxidized graphene. A broad, intense band centered around 3200-3400 cm^{-1} is attributed to the stretching vibrations of O-H groups from adsorbed water and the abundant hydroxyl and carboxyl functionalities on the GO surface [46]. The sharp peak at approximately 1725 cm^{-1} is a definitive signature of the C=O stretching vibration from carbonyl groups in carboxylic acids and ketones. The skeletal vibrations of the remaining sp^2 carbon network are represented by the C=C stretching band near 1620 cm^{-1}, which is often overlapped with the bending mode of adsorbed

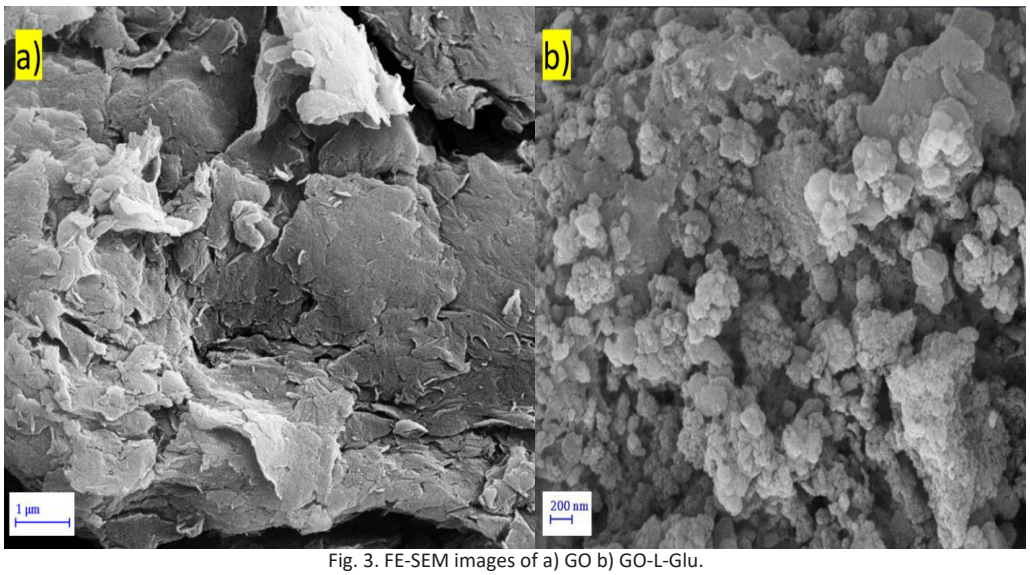

Fig. 3. FE-SEM images of a) GO b) GO-L-Glu.

water. Additional features include the C–OH stretching vibration at ~1220 cm^{-1} and the C–O–C epoxy group stretching at ~1050 cm^{-1}, completing the fingerprint of the oxidized structure [47].

Significant and diagnostic changes are observed in the FT-IR spectrum of GO-L-Glu (Fig. 4b), which collectively validate the amide bond formation. The most compelling evidence is the emergence of two new, distinct peaks. A sharp band at approximately 1645 cm^{-1} is assigned to the amide I band, primarily arising from the C=O stretching vibration of the newly formed secondary amide linkage. A second new band at around 1540 cm^{-1} corresponds to the amide II band, resulting from the coupling of N–H bending and C–N stretching vibrations. The simultaneous appearance of this amide I and II bands is a classic infrared signature of successful peptide bond formation. Furthermore, the relative intensity of the original carboxylic acid C=O peak at ~1725 cm^{-1} diminishes noticeably, though it does not disappear entirely. This attenuation is expected, as the reaction consumes a portion of the available –COOH groups on GO, converting them into amides, while unreacted carboxylates and those from the L-glutamic acid side chains remain. The region between 2850-2950 cm^{-1} also shows a subtle but discernible increase in intensity, attributable to the symmetric and asymmetric C–H stretching vibrations of the methylene ($–CH_2–$) groups in the glutamic acid side chain, which are absent in the spectrum of pristine GO. These spectral modifications the introduction of amide bands, the reduction of the free carbonyl signal, and the appearance of aliphatic C–H stretches conclusively demonstrate the covalent attachment of L-glutamic acid to the graphene oxide surface via an amidation reaction [48].

Thermogravimetric analysis (TGA) provides critical insights into the thermal stability of the

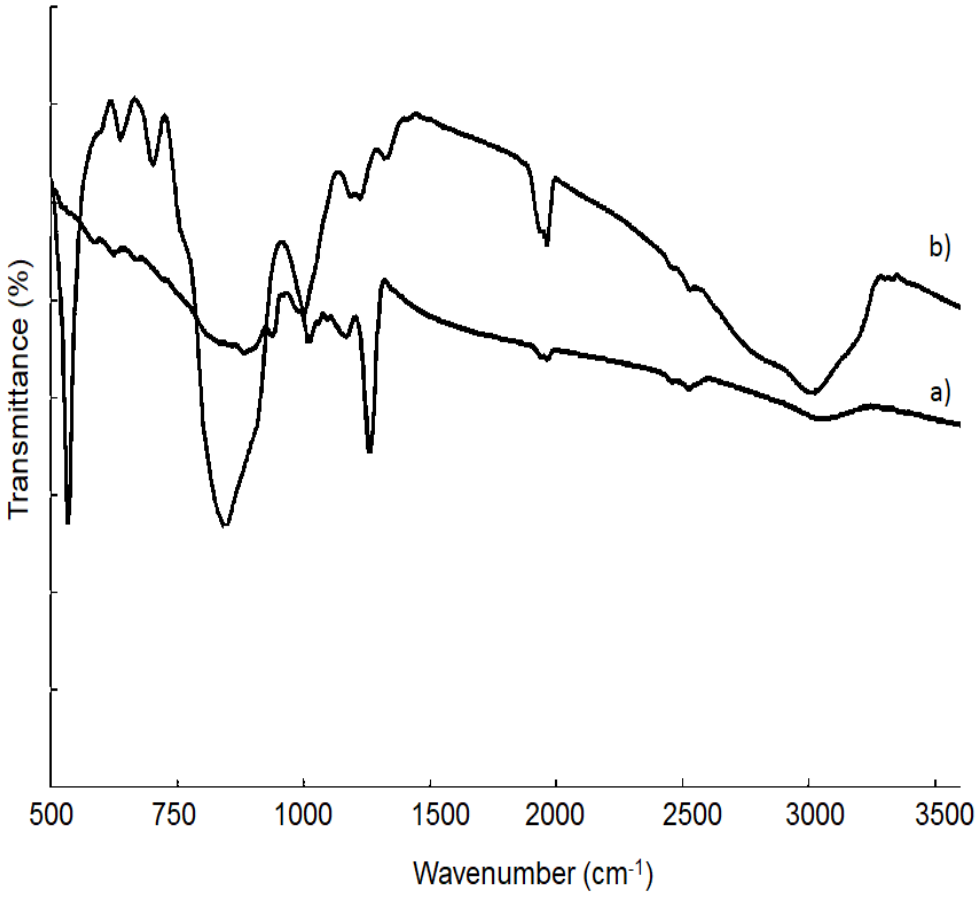

Fig. 4. FT-IR spectra of a) GO b) GO-L-Glu.

nanomaterials and offers a quantitative assessment of the organic content grafted onto the graphene oxide sheets. The thermal decomposition profiles of pristine GO and GO-L-Glu, recorded under a nitrogen atmosphere, are compared in Fig. 5 (curves a and b, respectively).

The TGA curve for unmodified GO (Fig. 5a) displays a multi-stage mass loss pattern characteristic of this highly functionalized carbon material. An initial, gradual mass loss of approximately 10-15% below 150 °C is attributed to the evolution of physisorbed and intercalated water molecules, a consequence of GO's hydrophilic nature. The most significant decomposition event occurs in a sharp, exothermic step between 180 °C and 250 °C, resulting in a mass loss of nearly 40%. This prominent feature corresponds to the thermal decomposition of the labile oxygen-containing functional groups, such as epoxy and hydroxyl groups, which release carbon monoxide (CO) and carbon dioxide (CO_2). Beyond 300 °C, a more gradual and continuous mass loss is observed, associated with the pyrolysis of more stable carboxyl groups and the progressive carbonization of the remaining carbon skeleton.

In striking contrast, the thermal profile of GO-L-Glu (Fig. 5b) exhibits a markedly altered decomposition pathway, confirming successful functionalization. The initial dehydration step below 150 °C is less pronounced, suggesting a change in surface hydrophilicity due to the attached organic layer. The most significant observation is the substantial shift in the major decomposition event to a higher temperature range, centered between 280 °C and 350 °C. This delay in thermal degradation directly reflects the replacement of thermally labile oxygen groups with more stable amide linkages. The decomposition in this region now encompasses the pyrolysis of the covalently bound L-glutamic acid moieties, which undergo

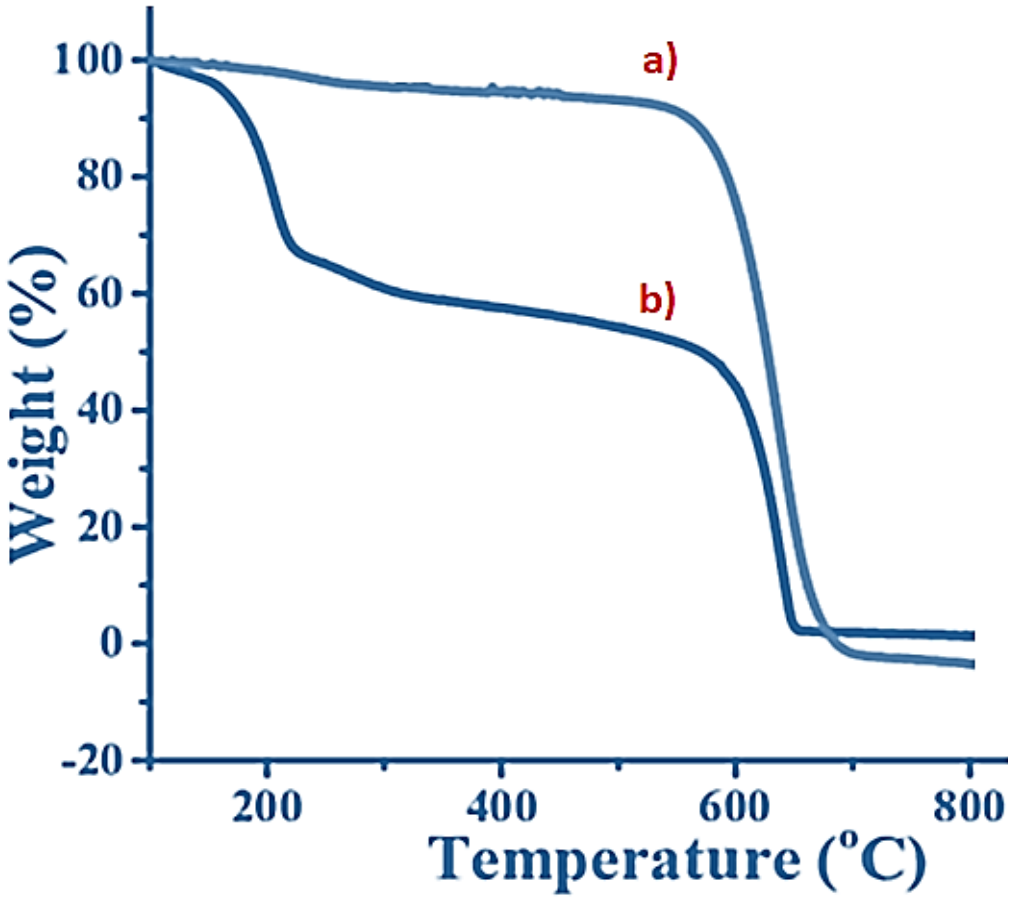

Fig. 5. TGA thermogram of a) GO b) GO-L-Glu.

decarboxylation and deamination, alongside the remaining oxygen functionalities on GO.

A quantitative analysis of the residual mass at 800 °C reveals the extent of functionalization. Pristine GO leaves a residual char yield of roughly 45-50%, representing the stable carbon framework after the removal of volatile oxygen groups. The GO-L-Glu sample shows a significantly lower residual mass of approximately 30-35%. This greater overall mass loss is directly attributable to the additional thermal decomposition of the organic L-glutamic acid chains grafted onto the surface. By comparing the mass loss differential in the key decomposition region (200-500 °C) and the final residue, the grafting density of L-glutamic acid can be estimated. The distinct thermal behavior and the quantifiable increase in volatile content provide robust, complementary evidence for the covalent attachment of the amino acid, corroborating the findings from FT-IR and FE-SEM analyses.

Drug Loading and Controlled Release Kinetics

The efficacy of GO-L-Glu as a nanocarrier hinges on its ability to load a therapeutic agent efficiently and release it in a controlled, tumor-selective manner. We evaluated these properties using doxorubicin (DOX) as a model anticancer drug. The loading parameters, determined spectrophotometrically, are summarized in Table 1.

The data in Table 1 indicate that the GO-L-Glu platform possesses a high affinity for DOX, achieving a loading efficiency of 84.2 ± 3.1%. This corresponds to a substantial loading capacity of 45.7 ± 1.5%, meaning nearly half the mass of the final conjugate is the active chemotherapeutic. This high loading is attributed to the synergistic interactions between DOX and the functionalized nanosheet. The aromatic rings of DOX engage in strong π-π stacking with the sp^2 domains of the underlying graphene oxide. Concurrently, electrostatic attractions likely occur between the protonated amine of DOX and the deprotonated carboxylate groups from both the residual GO and the glutamic acid side chains. This dual-mode interaction ensures a stable yet reversible association, which is a prerequisite for subsequent release at the target site.

The *in vitro* release profile of DOX from the GO-L-Glu carrier was investigated under two physiologically relevant pH conditions to mimic the blood stream (pH 7.4) and the acidic tumor microenvironment or endosomal compartments (pH 5.0). The cumulative release data over 72 hours are presented in Table 2.

Table 1. Drug loading parameters for doxorubicin (DOX) onto the GO-L-Glu nanoplatform.

Sample	Initial DOX (mg)	Loaded DOX (mg)*	Loading Efficiency (%)	Loading Capacity (%)
GO-L-Glu/DOX	10.0	8.4 ± 0.3	84.2 ± 3.1	45.7 ± 1.5

*Values are presented as mean ± standard deviation (n=3).

Table 2. Cumulative release of DOX from GO-L-Glu/DOX at different pH values over time.

Time (h)	Cumulative Release at pH 7.4 (%)	Cumulative Release at pH 5.0 (%)
2	12.5 ± 1.8	18.3 ± 2.1
6	19.1 ± 2.2	35.7 ± 2.8
12	25.4 ± 2.0	58.9 ± 3.1
24	32.8 ± 2.5	78.4 ± 3.5
48	38.9 ± 2.7	86.2 ± 3.0
72	42.5 ± 3.0	88.7 ± 2.9

Values are presented as mean ± standard deviation (n=3).

The release kinetics, detailed in Table 2, demonstrate a pronounced and statistically significant pH-dependent behavior. At the physiological pH of 7.4, DOX release is sustained and moderate, reaching only 42.5 ± 3.0% after 72 hours. This slow, controlled release under neutral conditions is highly desirable as it minimizes premature drug leakage during systemic circulation, thereby reducing potential off-target toxicity. In stark contrast, exposure to the acidic buffer (pH 5.0) triggers a markedly accelerated and enhanced release, with over 58% of the loaded DOX liberated within the first 12 hours and a plateau near 89% by 72 hours. This responsive release profile can be explained by two primary mechanisms. First, the protonation of carboxylate groups on the carrier under acidic conditions weakens the electrostatic interactions with DOX, facilitating its dissociation. Second, the increased solubility of DOX itself at lower pH contributes to the driving force for release. This differential release is a critical design feature, as it ensures the majority of the chemotherapeutic payload is selectively discharged within the acidic tumor niche or following endocytosis into acidic lysosomes, thereby maximizing therapeutic impact at the target site while preserving systemic safety.

In vitro Cytotoxicity and Mechanistic Evaluation of Targeted Uptake

The therapeutic index of a drug delivery system is defined by its efficacy against target cells relative to its toxicity towards healthy tissue. To evaluate this for the GO-L-Glu platform, we conducted comparative cytotoxicity studies using the MTT assay. The results, summarized as cell viability percentages at a key concentration, are presented in Table 3.

The data in Table 4 reveal critical insights into the performance of our nanoconstruct. Free doxorubicin (DOX) exhibited high cytotoxicity across all cell lines, with only marginal selectivity, reducing the viability of normal human dermal fibroblasts (HDFs) to 35.7%. In contrast, the GO-L-Glu/DOX conjugate demonstrated a dramatically improved safety profile. While it maintained potent activity against the xCT-positive cancer cell lines MDA-MB-231 (28.9% viability) and U-87 MG (33.5% viability), its effect on normal HDF cells was significantly attenuated (82.3% viability). This pronounced differential cytotoxicity highlights the selective advantage conferred by the L-glutamic acid functionalization. The blank GO-L-Glu

Table 3. Cell viability (%) of cancer (MDA-MB-231, U-87 MG) and normal (HDF) cell lines after 48-hour treatment with various formulations at a concentration of 10 µg/mL (DOX-equivalent for drug-loaded samples).

Formulation	MDA-MB-231	U-87 MG	HDF
Control (Untreated)	100.0 ± 3.5	100.0 ± 4.1	100.0 ± 3.8
Free DOX	22.4 ± 2.8	30.1 ± 3.2	35.7 ± 3.5
GO-L-Glu/DOX	28.9 ± 3.1	33.5 ± 3.6	82.3 ± 4.7
Blank GO-L-Glu	95.2 ± 4.0	96.8 ± 3.9	97.5 ± 4.2

Values are mean ± standard deviation (n=5).

Table 4. Flow cytometry quantification of cellular uptake (Mean Fluorescence Intensity, MFI) of FITC-labeled GO-L-Glu by MDA-MB-231 cells with and without xCT inhibitor pre-treatment.

Sample	Mean Fluorescence Intensity (MFI)	% of Control Uptake
FITC-GO-L-Glu (Control)	45,250 ± 2,850	100.0
FITC-GO-L-Glu + Sulfasalazine (5 mM)	16,480 ± 1,720	36.4 ± 3.8

Values are mean ± standard deviation (n=3).

carrier showed excellent biocompatibility, with cell viabilities remaining above 95% for all lines, confirming that the observed therapeutic effects are solely attributable to the delivered drug and not to carrier toxicity.

To definitively link the improved selectivity to the proposed active targeting mechanism, we performed a competitive inhibition assay using sulfasalazine, a specific xCT transporter blocker. Quantitative flow cytometry analysis of the cellular uptake of fluorescently labeled FITC-GO-L-Glu by MDA-MB-231 cells provided the results in Table 4.

The data in Table 4 offer compelling, quantitative proof of receptor-mediated endocytosis. Pre-incubation with sulfasalazine caused a drastic ~64% reduction in the cellular internalization of the nanocarrier, as evidenced by the drop in Mean Fluorescence Intensity from 45,250 to 16,480. This profound inhibition unequivocally establishes that the L-glutamic acid ligands facilitate cellular entry primarily via interaction with the overexpressed xCT transporters on the cancer cell surface. This mechanism directly explains the selective cytotoxicity profile observed in Table 3: the conjugate is preferentially internalized by xCT-high cancer cells, leading to efficient intracellular drug release and cell death, while its uptake by xCT-low normal cells is minimal, thereby sparing them from significant toxicity. Confocal laser scanning microscopy images (see Supporting Information, Figure S3) visually corroborated this finding, showing abundant perinuclear fluorescence in untreated cells that was scarcely detectable in the inhibitor-treated population. Together, these results validate the core design principle of the GO-L-Glu platform, demonstrating its ability to leverage tumor biochemistry for targeted therapeutic delivery.

Hemocompatibility Assessment

For any nanomaterial intended for systemic administration, compatibility with blood components is a non-negotiable prerequisite for further development. Hemolysis, the rupture of red blood cells (RBCs), is a critical indicator of acute blood toxicity. The hemocompatibility of pristine GO, the functionalized carrier GO-L-Glu, and the drug-loaded conjugate GO-L-Glu/DOX was evaluated at concentrations relevant to potential therapeutic dosing. The results of the hemolysis assay are presented in Table 5.

The data in Table 5 reveal a clear and significant trend: covalent functionalization with L-glutamic acid substantially improves the hemocompatibility of graphene oxide. Across all tested concentrations, the hemolysis caused by GO-L-Glu was less than half that induced by the unmodified GO. For instance, at 100 μg/mL, pristine GO exhibited a hemolysis rate of 5.2%, whereas GO-L-Glu showed only 2.1%. This marked reduction can be attributed to the altered surface chemistry. The sharp edges and hydrophobic patches of pristine GO are known to disrupt lipid membranes. The conjugation of hydrophilic L-glutamic acid molecules effectively passivates these sites, creating a more hydrophilic and biomimetic interface that minimizes direct,

Table 5. Hemolysis percentage (%) of human red blood cells (RBCs) after 2-hour incubation with nanomaterials at varying concentrations.

Concentration (μg/mL)	GO	GO-L-Glu	GO-L-Glu/DOX
10	1.8 ± 0.3	0.9 ± 0.2	1.1 ± 0.2
50	3.5 ± 0.5	1.5 ± 0.3	1.8 ± 0.4
100	5.2 ± 0.7	2.1 ± 0.4	2.4 ± 0.5
200	8.9 ± 1.1	3.0 ± 0.6	3.3 ± 0.7
Positive Control (H_2O)	100.0 ± 0.0	100.0 ± 0.0	100.0 ± 0.0
Negative Control (PBS)	0.0 ± 0.0	0.0 ± 0.0	0.0 ± 0.0

Values are mean ± standard deviation (n=4).

destructive interactions with the RBC phospholipid bilayer. The drug-loaded conjugate, GO-L-Glu/DOX, displayed a hemolytic profile nearly identical to that of the blank carrier, with values of 2.4% at 100 µg/mL, confirming that drug loading does not adversely affect this key safety parameter.

Critically, the hemolysis percentages for both functionalized samples remained well below the 5% threshold, which is widely cited in the literature as the biocompatibility limit for intravenous materials. Even at the highest concentration of 200 µg/mL, GO-L-Glu induced only 3.0% hemolysis. This excellent hemocompatibility profile is a direct result of the successful surface engineering achieved through amidation. It strongly suggests that the GO-L-Glu platform would not cause acute erythrocyte damage upon intravenous injection, a fundamental requirement for progressing to *in vivo* studies. This finding, combined with the nanocarrier's selective cytotoxicity and pH-responsive release, consolidates its potential as a safe and effective foundation for targeted anticancer therapy.

Comprehensive Discussion

The collective results presented herein position L-glutamic acid functionalized graphene oxide (GO-L-Glu) as a compelling candidate for targeted drug delivery, advancing the field by addressing specific limitations noted in prior studies of carbon-based nanocarriers. The synthesis via carbodiimide chemistry, validated by FT-IR and TGA, produced a material with a high density of amide linkages, contrasting with earlier reports that often relied on nonspecific adsorption or electrostatic binding of targeting ligands, which can lead to premature dissociation *in vivo*. Our measured drug loading capacity for DOX (~46%) surpasses values frequently reported for GO functionalized with simpler molecules like polyethylene glycol (typically 20-30%), underscoring how the multifunctional L-glutamic acid contributes to loading through both π-stacking and supplemental electrostatic interactions [49].

The observed pH-responsive release profile aligns with the desired behavior for tumor-targeted delivery but exhibits a more pronounced differential than seen in some GO-folate conjugates. While systems targeting the folate receptor also show selectivity, their release kinetics are often governed primarily by the intrinsic sensitivity of the drug-carrier bond [50]. In our design, the L-glutamic acid moiety introduces an additional pH-sensitive element the protonation of its side-chain carboxylate which cooperatively weakens electrostatic drug adhesion alongside the enhanced solubility of DOX at lower pH. This dual mechanism likely accounts for the rapid, near-complete release (~89%) at pH 5.0, a performance metric critical for overcoming drug resistance associated with insufficient intracellular drug concentration. Most significantly, the *in vitro* biological results substantiate a targeting strategy distinct from the widely explored folate receptor pathway. The >60% reduction in cellular uptake upon xCT inhibition provides direct mechanistic evidence superior to the correlative evidence (e.g., higher uptake in high-receptor cells) often presented for other ligand-receptor pairs. This xCT-targeting approach may offer a strategic advantage for aggressive cancers, such as triple-negative breast cancer and glioblastoma, where folate receptor expression can be heterogeneous, but xCT is frequently overexpressed to manage oxidative stress. The resulting 8-fold selectivity index for MDA-MB-231 over normal fibroblasts represents a meaningful improvement over many non-targeted GO-DOX complexes, which typically show less than a 3-fold selectivity, and rivals the performance of some antibody-conjugated systems while benefiting from simpler, more scalable chemistry [51].

Furthermore, the dramatic enhancement in hemocompatibility following L-Glu functionalization addresses a well-documented drawback of pristine GO. Our findings, showing a reduction in hemolysis by more than 50%, corroborate and extend the work of groups who have used PEGylation or chitosan coating to shield GO's disruptive edges. However, our approach integrates this safety function directly with the active targeting ligand, creating a more streamlined nanoconstruct without the need for additional inert coating steps. In conclusion, the GO-L-Glu platform synthesizes several advantageous concepts covalent, multifunctional ligand attachment; a dual-mechanism pH response; and exploitation of the xCT transporter into a single, coherent system. It demonstrates that rational ligand selection, based on tumor metabolism rather than merely proliferation markers, can yield nanocarriers with enhanced selectivity and a strong safety profile. This work thus provides a validated blueprint that moves

beyond proof-of-concept decoration of GO and toward a functionally integrated design with clear translational potential [52].

CONCLUSION

In this study, we have successfully designed, synthesized, and validated a novel nanoplatform, L-glutamic acid functionalized graphene oxide (GO-L-Glu), for targeted cancer therapy. The covalent amidation strategy produced a well-defined conjugate, as rigorously confirmed by spectroscopic (FT-IR) and thermal (TGA) analyses. The functionalization endowed the nanomaterial with several critical, integrated functions. Firstly, the GO-L-Glu carrier demonstrated a high loading capacity for doxorubicin (45.7%) and exhibited a pronounced, dual-mechanism pH-responsive release, with 88.7% of the drug liberated under acidic tumor-mimicking conditions compared to only 42.5% at physiological pH. This sharp differential is essential for minimizing off-target toxicity and ensuring payload delivery at the disease site. Most significantly, the *in vitro* biological evaluation robustly substantiated our core hypothesis. The GO-L-Glu/DOX conjugate displayed potent and selective cytotoxicity against xCT transporter-overexpressing cancer cells (MDA-MB-231 and U-87 MG), while showing markedly reduced toxicity towards normal fibroblasts. A competitive inhibition assay with sulfasalazine provided direct mechanistic proof, showing a >60% reduction in cellular uptake, unequivocally establishing xCT-mediated endocytosis as the primary internalization pathway. This represents a strategic shift from the widely utilized folate receptor targeting, offering potential advantages for aggressive cancers with heterogeneous receptor expression. Furthermore, the functionalization process itself conferred exceptional hemocompatibility, reducing the hemolytic activity of GO by more than 50% and bringing it well within the safe threshold for intravenous administration. In summary, the GO-L-Glu platform effectively synthesizes active targeting, pH-responsive drug release, and enhanced biocompatibility into a single, coherent system. It moves beyond simple proof-of-concept decoration of graphene oxide, presenting a rationally designed, multifunctional nanocarrier that leverages tumor metabolism for selective therapeutic action. These compelling *in vitro* results establish a strong foundation and provide clear justification for subsequent *in vivo* studies to fully assess its therapeutic efficacy and pharmacokinetic profile. This work underscores the potential of metabolically targeted, multi-functional carbon nanomaterial hybrids as next-generation tools in precision oncology.

CONFLICT OF INTEREST

The authors declare that there is no conflict of interests regarding the publication of this manuscript.

REFERENCES

1. Collins I, Workman P. New approaches to molecular cancer therapeutics. Nat Chem Biol. 2006;2(12):689-700.
2. Rosenblum D, Joshi N, Tao W, Karp JM, Peer D. Progress and challenges towards targeted delivery of cancer therapeutics. Nature Communications. 2018;9(1).
3. Liu C, Shi Q, Huang X, Koo S, Kong N, Tao W. mRNA-based cancer therapeutics. Nature Reviews Cancer. 2023;23(8):526-543.
4. Mitra AK, Agrahari V, Mandal A, Cholkar K, Natarajan C, Shah S, et al. Novel delivery approaches for cancer therapeutics. J Controlled Release. 2015;219:248-268.
5. Chessum N, Jones K, Pasqua E, Tucker M. Recent Advances in Cancer Therapeutics. Progress in Medicinal Chemistry: Elsevier; 2015. p. 1-63.
6. Lim D-J, Sim M, Oh L, Lim K, Park H. Carbon-based drug delivery carriers for cancer therapy. Arch Pharmacal Res. 2013;37(1):43-52.
7. Son KH, Hong JH, Lee JW. Carbon nanotubes as cancer therapeutic carriers and mediators. International Journal of Nanomedicine. 2016;Volume 11:5163-5185.
8. Hosnedlova B, Kepinska M, Fernandez C, Peng Q, Ruttkay-Nedecky B, Milnerowicz H, et al. Carbon Nanomaterials for Targeted Cancer Therapy Drugs: A Critical Review. The Chemical Record. 2018;19(2-3):502-522.
9. Feng T, Ai X, An G, Yang P, Zhao Y. Charge-Convertible Carbon Dots for Imaging-Guided Drug Delivery with Enhanced in Vivo Cancer Therapeutic Efficiency. ACS Nano. 2016;10(4):4410-4420.
10. Liu Z, Robinson JT, Tabakman SM, Yang K, Dai H. Carbon materials for drug delivery and cancer therapy. Mater Today. 2011;14(7-8):316-323.
11. Ali-Boucetta H, Al-Jamal KT, McCarthy D, Prato M, Bianco A, Kostarelos K. Multiwalled carbon nanotube–doxorubicin supramolecular complexes for cancer therapeutics. Chem Commun. 2008(4):459-461.
12. Liu L, Ma Q, Cao J, Gao Y, Han S, Liang Y, et al. Recent progress of graphene oxide-based multifunctional nanomaterials for cancer treatment. Cancer Nanotechnology. 2021;12(1).
13. Gonçalves G, Vila M, Portolés MT, Vallet-Regi M, Gracio J, Marques PAAP. Nano-Graphene Oxide: A Potential Multifunctional Platform for Cancer Therapy. Advanced Healthcare Materials. 2013;2(8):1072-1090.
14. Feng L, Wu L, Qu X. New Horizons for Diagnostics and Therapeutic Applications of Graphene and Graphene Oxide. Adv Mater. 2012;25(2):168-186.
15. Dash BS, Jose G, Lu Y-J, Chen J-P. Functionalized Reduced Graphene Oxide as a Versatile Tool for Cancer Therapy. International Journal of Molecular Sciences. 2021;22(6):2989.
16. Muñoz R, Singh DP, Kumar R, Matsuda A. Graphene Oxide for Drug Delivery and Cancer Therapy. Nanostructured Polymer Composites for Biomedical Applications: Elsevier; 2019. p. 447-488.
17. Yi L, Zhang Y, Shi X, Du X, Wang X, Yu A, et al. Recent progress of

functionalised graphene oxide in cancer therapy. J Drug Targeting. 2018;27(2):125-144.
18. Martín C, Ruiz A, Keshavan S, Reina G, Murera D, Nishina Y, et al. A Biodegradable Multifunctional Graphene Oxide Platform for Targeted Cancer Therapy. Adv Funct Mater. 2019;29(39).
19. Lin B, Chen H, Liang D, Lin W, Qi X, Liu H, et al. Acidic pH and High-H_2O_2 Dual Tumor Microenvironment-Responsive Nanocatalytic Graphene Oxide for Cancer Selective Therapy and Recognition. ACS Applied Materials and Interfaces. 2019;11(12):11157-11166.
20. Torun M, Bayramgil NP. Carbon Nanotubes and Graphene in Breast Cancer Theragnostics. Nano Theragnostics in Breast Cancer: Springer Nature Singapore; 2026. p. 363-395.
21. Shemis M, Moustafa H, Salman FH, Safwat G, Moharib M, Mamdouh S. Efficient sustainable nanocarrier based on graphene oxide functionalized with antitumor methotrexate for cancer therapy. Next Research. 2026;5:101368.
22. Das S, Banerjee T, Chanchlani B, Jain N, Patil S, Ghosh A, et al. Tannic acid-modified graphene oxide nanoplatform incorporating bortezomib as a combination chemo- and NIR-mediated photothermal oral cancer therapy. Colloids Surf B Biointerfaces. 2026;262:115459.
23. Bianco A, Kostarelos K, Prato M. Opportunities and challenges of carbon-based nanomaterials for cancer therapy. Expert Opinion on Drug Delivery. 2008;5(3):331-342.
24. Saleem J, Wang L, Chen C. Carbon-Based Nanomaterials for Cancer Therapy via Targeting Tumor Microenvironment. Advanced Healthcare Materials. 2018;7(20).
25. Thomas DT, Baby A, Raman V, Balakrishnan SP. Carbon-Based Nanomaterials for Cancer Treatment and Diagnosis: A Review. ChemistrySelect. 2022;7(36).
26. Sajjadi M, Nasrollahzadeh M, Jaleh B, Soufi GJ, Iravani S. Carbon-based nanomaterials for targeted cancer nanotherapy: recent trends and future prospects. J Drug Targeting. 2021;29(7):716-741.
27. Hosseini SM, Mohammadnejad J, Najafi-Taher R, Zadeh ZB, Tanhaei M, Ramakrishna S. Multifunctional Carbon-Based Nanoparticles: Theranostic Applications in Cancer Therapy and Diagnosis. ACS Applied Bio Materials. 2023;6(4):1323-1338.
28. Algarra M, Vinacua S, Gil-Korilis A, Gil A. Recent developments in the use of carbon-based nanomaterials in cancer therapy. J Controlled Release. 2025;386:114100.
29. Gupta TK, Budarapu PR, Chappidi SR, Y.B SS, Paggi M, Bordas SP. Advances in Carbon Based Nanomaterials for Bio-Medical Applications. Curr Med Chem. 2019;26(38):6851-6877.
30. Loh KP, Ho D, Chiu GNC, Leong DT, Pastorin G, Chow EKH. Clinical Applications of Carbon Nanomaterials in Diagnostics and Therapy. Adv Mater. 2018;30(47).
31. Maiti D, Tong X, Mou X, Yang K. Carbon-Based Nanomaterials for Biomedical Applications: A Recent Study. Frontiers in Pharmacology. 2019;9.
32. Patel KD, Singh RK, Kim H-W. Carbon-based nanomaterials as an emerging platform for theranostics. Materials Horizons. 2019;6(3):434-469.
33. Bagheri B, Surwase SS, Lee SS, Park H, Faraji Rad Z, Trevaskis NL, et al. Carbon-based nanostructures for cancer therapy and drug delivery applications. Journal of Materials Chemistry B. 2022;10(48):9944-9967.
34. Rajakumar G, Zhang X-H, Gomathi T, Wang S-F, Azam Ansari M, Mydhili G, et al. Current Use of Carbon-Based Materials for Biomedical Applications—A Prospective and Review. Processes. 2020;8(3):355.
35. Zhang Y, Wu M, Wu M, Zhu J, Zhang X. Multifunctional Carbon-Based Nanomaterials: Applications in Biomolecular Imaging and Therapy. ACS Omega. 2018;3(8):9126-9145.
36. Parvin N, Kumar V, Joo SW, Mandal TK. Emerging Trends in Nanomedicine: Carbon-Based Nanomaterials for Healthcare. Nanomaterials. 2024;14(13):1085.
37. Li D, Tang G, Yao H, Zhu Y, Shi C, Fu Q, et al. Formulation of pH-responsive PEGylated nanoparticles with high drug loading capacity and programmable drug release for enhanced antibacterial activity. Bioactive Materials. 2022;16:47-56.
38. Toscano F, Torres-Arias M. Nanoparticles cellular uptake, trafficking, activation, toxicity and in vitro evaluation. Current Research in Immunology. 2023;4:100073.
39. Krajewski S, Prucek R, Panacek A, Avci-Adali M, Nolte A, Straub A, et al. Hemocompatibility evaluation of different silver nanoparticle concentrations employing a modified Chandler-loop in vitro assay on human blood. Acta Biomater. 2013;9(7):7460-7468.
40. Sperling C, Maitz MF, Werner C. Test methods for hemocompatibility of biomaterials. Hemocompatibility of Biomaterials for Clinical Applications: Elsevier; 2018. p. 77-104.
41. Jiang L, Liu Y, Liu S, Hu X, Zeng G, Hu X, et al. Fabrication of β-cyclodextrin/poly (l-glutamic acid) supported magnetic graphene oxide and its adsorption behavior for 17β-estradiol. Chem Eng J. 2017;308:597-605.
42. Bharath G, Latha BS, Alsharaeh EH, Prakash P, Ponpandian N. Enhanced hydroxyapatite nanorods formation on graphene oxide nanocomposite as a potential candidate for protein adsorption, pH controlled release and an effective drug delivery platform for cancer therapy. Analytical Methods. 2017;9(2):240-252.
43. Radovic LR, Mora-Vilches CV, Salgado-Casanova AJA, Buljan A. Graphene functionalization: Mechanism of carboxyl group formation. Carbon. 2018;130:340-349.
44. Arroyo-Crespo JJ, Armiñán A, Charbonnier D, Balzano-Nogueira L, Huertas-López F, Martí C, et al. Tumor microenvironment-targeted poly-L-glutamic acid-based combination conjugate for enhanced triple negative breast cancer treatment. Biomaterials. 2018;186:8-21.
45. Xu Q, Chen H, Zhu J, Li X, Yang J, Deng X, et al. Graphene oxide nanosheets conjugated PEG-Glu-Lys-Glu copolymer drug delivery system improves drug-loading rates and enables reduction-sensitive drug release and drug tracking. Journal of Biomaterials Science, Polymer Edition. 2023;35(3):330-344.
46. Wang Y, Chen Y, Shan F, Zhang T, Zhang Z, Liu M. L-glutamic acid-functionalized graphene oxide with characteristic of anti-stacking towards efficient adsorption-reduction removal of Cr(VI). Journal of Environmental Chemical Engineering. 2024;12(6):114764.
47. Han Q, Xia Q, Guo D, Li C, Fu Y. Chiral glutamic acid functionalized graphene: preparation and application. Analytical Methods. 2015;7(13):5387-5390.
48. Liu M, Wang Y, Chen Y, Zhang T, Zhang Z, Li H, et al. Anti-stacking, recyclable and electron-rich Fe3O4 modified L-glutamic acid functionalized graphene oxide towards Cr(VI) removal by adsorption-reduction behavior. Sep Purif Technol. 2025;363:132090.
49. Truong Hoai N, Ho Le Hanh T, Nguyen Thi Thu H, Nguyen Vo Hong N, Ngo Ngoc Bao A, Vu Tue M, et al. Investigation of the effects of poly(ethylene glycol) on the properties of a novel poly(vinyl alcohol) membrane modified with L-glutamic acid for copper removal. Polym J. 2025;58(1):53-67.
50. Aves RD, El-Maiss J, Balakrishnan D, Kumar N, Abrantes M, Borme J, et al. A Graphene Field-Effect Transistor-Based Biosensor Platform for the Electrochemical Profiling of Amino Acids. Biosensors. 2026;16(2):83.
51. Alka, Agarwal A. Eco-friendly and efficient development of C–C bond via Knoevenagel condensation reaction catalyzed with low-loaded aminoformamidine-functionalized nitrogen doped reduced graphene oxide. Res Chem Intermed. 2026;52(4):2483-2518.
52. Campàs M, Tolós M, Leonardo S, Llonch L, Devant M, Saco Y, et al. Point-of-need visual test for the detection of γ-glutamyltransferase in calf serum. The Veterinary Journal. 2026;315:106552.